COMPARISON OF EXTRUDED AND PRESSED LOW COST CERAMIC MICROFILTRATION MEMBRANES

Lorente-Ayza, M-M.[a],*, Mestre, S.[a], Menéndez, M.[b], Sánchez, E. [a]

[a] *Instituto Universitario de Tecnología Cerámica. Universitat Jaume I. Castellón (Spain)*
[b] *Instituto de Investigación en Ingeniería de Aragón. Universidad de Zaragoza (Spain)*

**Corresponding Author*

Abstract

A comparison has been made between ceramic microfiltration membranes of the same composition obtained by pressing and by extrusion in terms of microstructure and properties.

The extruded membranes displayed lower porosity and smaller pore size than pressed membranes. The higher the clay content in the starting composition, the clearer this tendency became. In contrast, the difference tended to disappear when starch was added to the initial composition. The mechanical strength values followed a decreasing exponential variation with porosity, which was influenced by the starting composition and the shaping method.

Water permeability reflected the strong effect of the mean pore size. The membranes synthesised from the composition with the higher clay content showed the lowest permeability, while those obtained from the composition including starch showed the highest value. A model derived from the Hagen-Poiseuille equation enabled the tortuosity values to be calculated.

Keywords: membrane; shaping; porosity; permeability; tortuosity.

1 Introduction

Ceramic membranes offer unique advantages due to their good properties, such as mechanical strength, thermal stability and resistance to harsh chemical conditions (pH extremes, oxidizing agents...). However, their high cost has traditionally limited their use in cost sensitive processes such as environmentally related applications [1]–[3].

The composition of ceramic membranes in industry is usually based on alumina, zirconia, titania or a combination of these oxides. In particular, a substantial number of papers have been published concerning membranes fabricated using α-alumina. If ceramic membranes of low cost and acceptable performance were available, they could be used in a larger number of processes such as tertiary water treatment, membrane bioreactors, separation and purification operations, etc. For this reason, significant efforts have been made in recent years in membrane technology to develop new porous ceramic materials based on locally available low cost raw materials such as clay, kaolin, zeolite, bauxite, diatomite, andalusite, etc. [4]–[12]. These materials are available in abundance and require sintering temperatures that are significantly lower than those needed for metal oxide-based materials. As recognised in the literature, a dramatic cost reduction in ceramic manufacturing can be expected by replacing the more expensive raw materials by these minerals in ceramic membranes [13]. Thus, replacing alumina by kaolin can reduce the raw material costs by a factor of up to 100. Significant economic reductions can also be gained by decreasing the sintering temperature for alumina-based compositions from 1600 ºC to the common sintering

temperature of 1200 ºC for whiteware ceramics. Therefore, the development of mineral-based ceramic membranes could lead to a new technological revolution that would add great economic value to natural minerals that are widely available all over the world as well as to ceramic manufacturing companies that process these raw materials.

Mullite-based ceramic membranes represent one of the best alternatives to α-alumina due to their outstanding properties such as low thermal conductivity and expansion, excellent creep resistance and considerable thermal, chemical and mechanical stability. To produce the required amount of mullite phase, clayey minerals must necessarily be included in the starting composition. As a consequence, research into the use of clays and kaolin as membrane materials has attracted much attention in recent years [4], [9], [13]–[22]. Moreover, these macroporous membranes have been applied for various separation applications, such as separation of salt, dye, heavy metals, oil emulsion and proteins [16]–[24]. However, these prepared clayey membranes have shown some shortcomings: low porosity, small pore size, low strength or large shrinkage resulting from the fact that clay can be easily sintered from the action of various existing impurities [25], [26]. A common strategy to augment porosity and pore size involves the use of organic pore formers such as starch derivatives [4], [20], [27]–[29]. On the other hand, the addition of minerals supplying alkaline-earth metals (mainly Mg and Ca) to the starting composition, such as wollastonite, calcite or dolomite, can contribute to a reduction in the sintering temperature and soaking time as well as to an increase in the strength of the ceramic membrane. Besides, alkaline-earth carbonates (calcite and dolomite) have also been used as pore formers. Nevertheless, the decomposition of calcium or calcium-magnesium carbonates can produce a two-fold effect since at low temperatures (<1000 ºC) large pores are formed which turn into smaller ones at higher temperatures (>1300 ºC) as a consequence of the liquid phase sintering mechanism [30]–[32]. Recently, Harabi et al demonstrated that adding calcium carbonate to a kaolin-based ceramic composition allows mullite-based ceramics to be obtained without the undesirable cristobalite phase [13].

The starting composition is the main factor that defines the sintering profile as well as the membrane microstructure and cost. However, the method of membrane fabrication decides the final product geometry. Ceramic membranes are currently available in different configurations. There are two distinct groups: flat disc- and tubular-shaped, and the latter clearly dominates the field [4], [13], [33]. Other more complicated configurations such as multichannel monoliths (honeycomb) and hollow-fibre modules can be considered as tubular variations. Most membranes (commercial and homemade) are fabricated by powder pressing and mainly by paste processing (extrusion) because this last method is much more suitable for tubular and multichannel configurations. Although previous research on ceramic membranes has indiscriminately used powder pressing and extrusion as well as other colloidal processing methods to form ceramic membranes, no previous publications have been found in which the influence of the shaping method for a given (low cost) ceramic membrane has been examined. This is because in many cases the ceramic compositions in terms of the nature and quantity of raw materials and additives must be adapted to a specific shaping method, as recently reported [13]. However, the strong impact of the ceramic forming on the microstructure and consequently on the final product properties and performance is widely accepted in other ceramic manufacturing processes [34]–[36].

Given the background described above, this work addresses the development of low cost ceramic membranes based on raw materials typically used in the ceramic industry, such as clay and calcium carbonate (an inorganic pore former) together with starch as

an organic pore former. The membranes have been formed by pressing and extrusion. The main objective of the work is to compare the microstructure and properties of the ceramic membranes obtained by using these two shaping methods with the same low cost ceramic compositions, in order to relate the starting composition and the shaping method with the membrane microstructure and properties. In addition, a tentative simple model to calculate the tortuosity has been proposed.

2 Experimental

2.1 Raw materials and membrane synthesis

Three inorganic raw materials were used to prepare low cost ceramic membranes: a Spanish clay mixture, calcite (OMYACARB 5-BE, Omya AG, Spain) and chamotte taken from fired tile scraps. All these raw materials are used in the tile manufacturing industry in Spain. The raw materials were dry milled in a ball mill until practically no particles over 60 μm mesh were left. Finally, potato starch (Roquette Freres S.A., France) was used in some of the compositions as an organic pore former. Table 1 shows the chemical and mineralogical composition of these materials. Figure 1 describes the particle size distribution of the three ground inorganic materials obtained with a laser diffraction particle size analyser (Mastersizer 2000, Malvern Instruments Ltd. UK). The mean particle size of the starch was 46 μm.

Table 1. Chemical and mineralogical compositions of the raw materials used (wt %).

	Clay	Calcite	Chamotte
SiO_2	67.2	0.24	70.1
Al_2O_3	20.3	0.15	20.4
Fe_2O_3	1.1	0.02	1.7
CaO	0.4	55.7	0.5
MgO	0.5	0.14	0.4
Na_2O	0.2	-	4.3
K_2O	3.0	0.01	2.0
TiO_2	1.0	-	0.7
Loss on ignition	6.3	43.7	-
Mineralogical composition	Kaolinite, Quartz; Albite, Microcline (potassic feldspar) Muscovite, Hematite	Calcite	Quartz, Albite, Microcline, Hematite

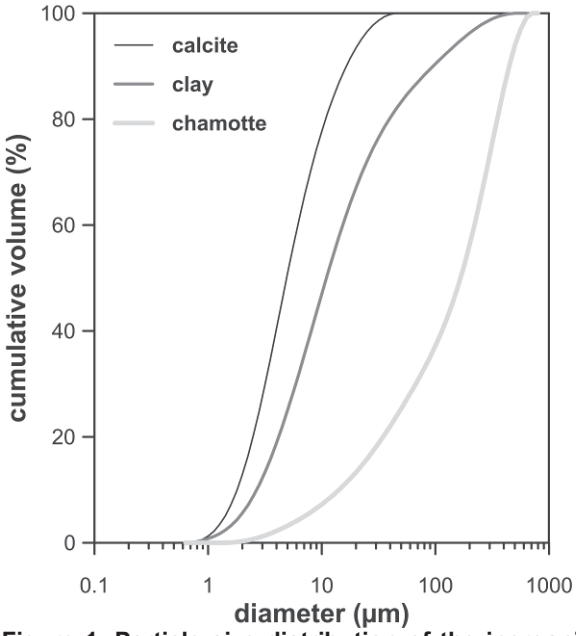

Figure 1. Particle size distribution of the inorganic raw materials used in this work after dry ball milling.

From these materials, three compositions were formulated as shown in table 2. Composition 1 was the reference mixture (standard composition), since it was made up of clay (mullite precursor), calcite (inorganic pore former) and chamotte as a filler. From this standard composition two other mixtures were developed. Composition 2 had a higher percentage of clay and a total absence of chamotte in order to increase the amount of colloidal particles, and thus a low permeability membrane could be expected. In contrast, in composition 3 lower percentages of clay as well as a given amount of starch were used in order to obtain a highly permeable membrane.

Table 2. Ceramic membrane compositions prepared in this work (wt %).

Ref.	Clay	Calcite	Chamotte	Potato starch
1	60	20	20	-
2	85	15	-	-
3	40	20	20	20

Ceramic membranes from compositions 1, 2 and 3 were formed by powder dry pressing and plastic extrusion following the procedure depicted in figure 2. The ceramic membranes were discs of 50 mm diameter and 7-10 mm thickness (7 mm for pressed pieces and 10 mm for extruded pieces). The powder pressing took place in a laboratory unidirectional press (Model Mignon, Nannetti,S.r.l., Italy) and the extrusion in a laboratory screw extruder (Model 050C, Talleres Felipe Verdés, S.A., Spain). The final reference for the ceramic membranes was related to the given composition and the shaping method. Thus compositions 1, 2 and 3 were given the serial references P1, P2 and P3 for the specimens obtained by pressing and E1, E2 and E3 for the ceramic membranes formed by extrusion.

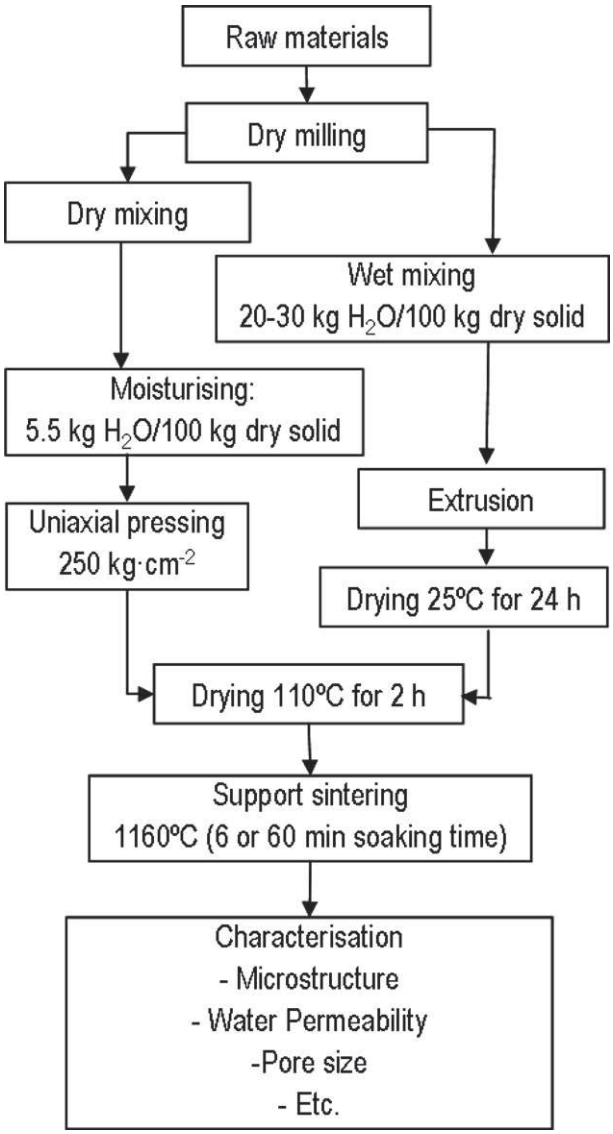

Figure 2. Procedures followed and process variables used to obtain ceramic membranes by powder pressing and extrusion.

The porosity of the dry pieces of the three compositions obtained by the two shaping methods was calculated by bulk density determination (Archimedes method) and true density measurements (helium picnometer, Ultrapycnometer 1000, Quantachrome Inc. USA).

Dry specimens obtained from both shaping methods and all the compositions were sintered in a laboratory electric kiln (Model Rapido, Pirometrol S.L., Spain) following different thermal cycles as shown in figure 3. The dwell time at maximum temperature (1160 ºC) was in all cases 60 min except for the standard composition 1 (P1 and E1 bodies) for which a shorter dwell time of 6 min was also tested with the aim of analysing the influence of the sintering time on the membrane characteristics. As observed in figure 3, the main difference between the thermal treatments of the three compositions is that the compositions containing starch were heated at a much lower rate, so as to preserve the integrity of the ceramic specimens during starch burnout. These sintering cycles were optimised after many preliminary tests.

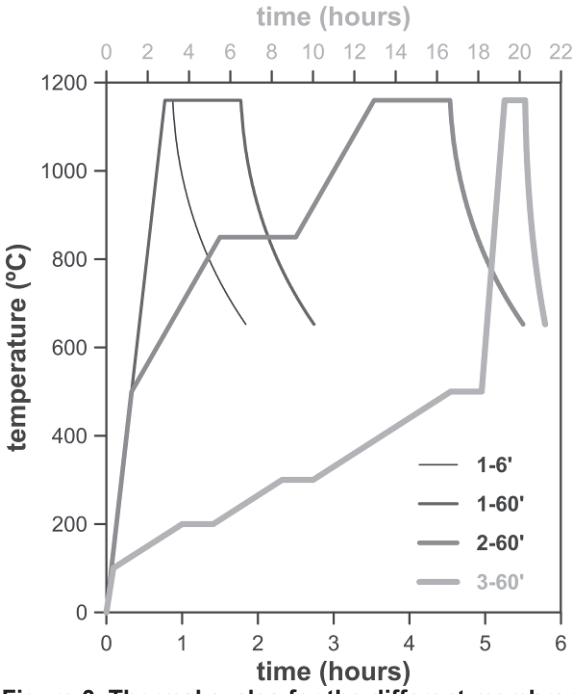

Figure 3. Thermal cycles for the different membrane samples of series P or E with a dwell time at maximum sintering temperature of 60 min (also 6 min for composition 1).

2.2 Sintered membranes characterization

The mineralogical composition of the membranes was determined by the XRD technique (Bruker, Theta-Theta D8 Advance, Germany). Pore size distribution was measured by mercury intrusion porosimetry (AutoPore IV 9500 Micromeritics, USA). The average pore size (d50) and open porosity (accessible to mercury intrusion) were calculated. Some sintered specimens were also examined by electron microscopy (FEG-ESEM Quanta 200F, FEI, USA) on cross-sectional surfaces of the samples. Micrographs were obtained using the back-scattered electron mode.

Mechanical strength was determined by a 3-point bending test in a universal testing machine (Model 4507, Instron, Massachusetts, USA). To carry out this test, sintered prismatic specimens with approximate dimensions of 80x20x10 mm were obtained. The procedures followed to obtain these specimens by pressing and extrusion were the same as those set out in figure 2. The experiments were performed at a constant strain rate of 5 mm/min. Ten test specimens were broken for each sample and the results were averaged.

The functionality of the membranes was assessed in terms of water permeability measurements carried out by means of a water permeameter specifically designed for disc configuration samples. Figure 4 shows a picture of the water permeameter with its main components: membrane holder (1), pressure gauge (2), valves (3, 4), feed inlet duct (5), permeate outlet duct (6). The water pressure applied to the membrane was varied from 0 to 6 bars while the water flow through the membrane disc was determined for a given time. From a direct application of Darcy's law, the permeability constant can be calculated according to equation 1, where K_p is the water permeability constant (m^2), μ is the water viscosity (0.001 kg m^{-1} s^{-1} at 20ºC and 1atm), E is the membrane thickness (m), slp is the slope of the straight line fit based on Darcy's law (m^3 s^{-1} Pa^{-1}), and A is the water permeation area (area of the chamber section where the membrane is placed in m^2).

$$K_p = \frac{slp \cdot \mu \cdot E}{A} \qquad \text{Eq. 1}$$

If the flux values obtained are represented against the applied pressure, a straight line may be obtained and the corresponding slope calculated. The K_p value determined for the membrane under study is obtained when the slope value is included in the Darcy's law [37]. Nevertheless, the water permeability values were recalculated in ($L \cdot h^{-1} \cdot m^{-2} \cdot bar^{-1}$) units for a better comparison with commercial membrane data [38].

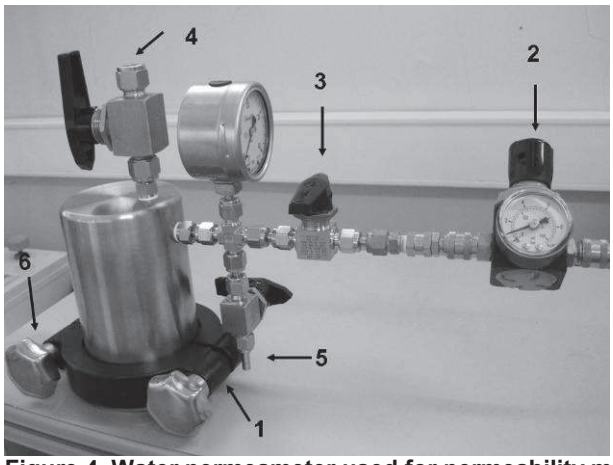

Figure 4. Water permeameter used for permeability measurements of the disc membranes.

3 Results and discussion

3.1 Porosity values of unfired membrane specimens

The porosity values of unfired bodies represent a good indicator of the feasibility of a given shaping method to form consistent ceramic specimens. This is particularly relevant in ceramic membranes since both inorganic and organic raw materials may be included in the starting compositions. The unfired porosity values (ε) ranged from 28 to 31% for the P series (ε_P) and from 27 to 31% for the E series (ε_E). These values are consistent with other ceramic specimens obtained by pressing or extrusion processes [35]. For the sake of a more understandable comparison, figure 5 plots the P specimen porosity/E specimen porosity ratio for the three compositions ($\varepsilon_P/\varepsilon_E$), together with the porosity of each series. As can be observed, the porosity values of the extruded pieces were slightly lower than those of the pressed bodies. This difference can be attributed to the plastic properties of the clay, which readily forms a paste and can be easily extruded to the desired shape with lower extrusion pressure. Nevertheless, the amount of clay in the three compositions also facilitated the powder flow during pressure compaction. As can be observed, composition 3 shows the least difference between the extruded and pressed bodies, due to the plasticity-decreasing effect produced by the starch [28], [39].

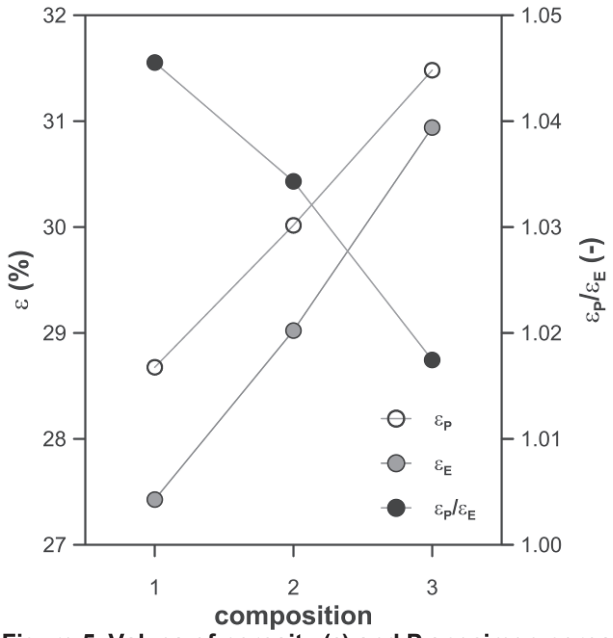

Figure 5. Values of porosity (ε) and P specimen porosity(ε_P)/E specimen porosity(ε_E) ratio for the three studied membrane compositions.

3.2 Membrane physical characterization

The major crystalline phases present in all the membranes were undissolved quartz, wollastonite and anorthite, independently of the shaping method (Figure 6 shows the XRD pattern of ceramic membrane samples obtained by pressing). These are the expected crystalline phases when a mixture of clay and calcium carbonate is sintered at high temperatures (>1100ºC) [13], [32], [40]. The amount of the calcium silicate (wollastonite) and aluminosilicate (anorthite) phases mainly depends on the relative amount of aluminium, calcium and silicon oxides in the starting composition. Mullite also develops during sintering, but the amount is much lower as a consequence of the small proportion of aluminium oxide in the starting composition and the relatively low sintering temperatures. For the P1 composition, the amount of crystalline phases (estimated from the height of the peaks) seems to decrease when a longer soaking time is applied at maximum temperature, this being a consequence of the longer time available for the dissolution of the crystals in the liquid phase. This explanation is confirmed by the decrease in the quartz signal when the sintering time was increased.

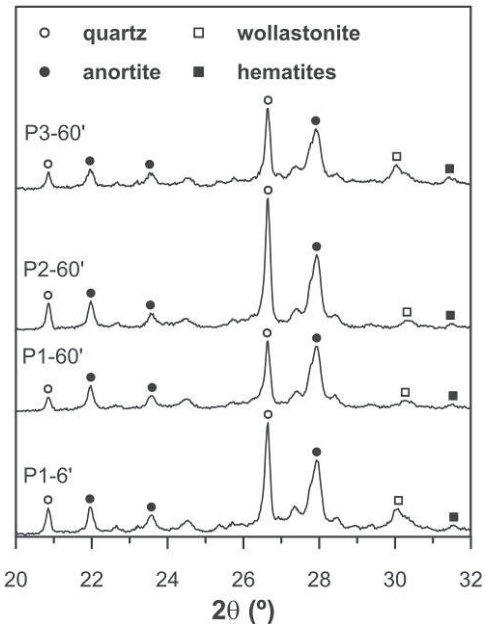

Figure 6. XRD patterns of ceramic membrane samples obtained by pressing (P1, P2, P3 series). Membrane P1 patterns are shown for the two dwell times (6 and 60 min) at maximum temperature.

Pore size distributions of the two series of samples are shown in figure 7a (P samples) and 7b (E samples). As expected, the P1 and E1 pieces sintered at the two dwell times at the maximum sintering temperature display lower porosity (related to the area inside the curve) and coarser pore sizes when sintered at a longer soaking time. These effects are a consequence of the sintering process, which takes place in the presence of the liquid phase provided by the alkaline and alkaline-earth oxide content in the starting raw materials. In addition, as extensively reported in the literature, the addition of starch substantially increases the porosity and shift pore size distribution of the sintered membranes to coarser pore size due to the burnout of the starch during the firing process, regardless of the forming process (pressing or extrusion) [20], [28], [41]–[45]. Finally, it was also observed that increasing the amount of clay in the composition (P2 and E2 against P1 and E1, respectively) drastically decreased the pore size (curves shift to the left) as a consequence of the higher amount of colloidal particles provided by the clay. Again, this occurred for both forming processes.

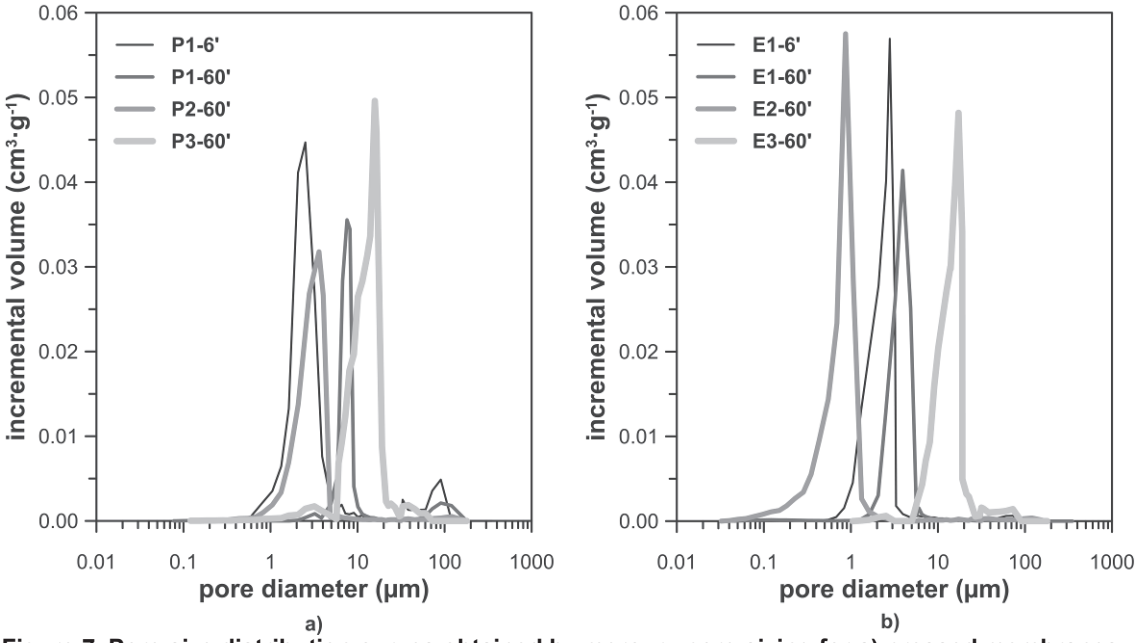

Figure 7. Pore size distribution curves obtained by mercury pore sizing for a) pressed membranes (P series) and b) extruded membranes (E series). Note that the P1 and E1 specimens were sintered at two dwell times (6 and 60 min).

To better understand the comparison between the microstructures of the P and E specimens, two new ratios were calculated: i) mean pore size (d_{50}) of P pieces/mean pore size (d_{50}) of E pieces and ii) open porosity (accessible to mercury) of P pieces/open porosity of E pieces. Figure 8 plots the values of these two ratios for the two series of bodies sintered at 60 min dwell time. The membranes obtained by extrusion displayed smaller pore sizes than those of the samples sintered from pressed bodies (the pore size distribution curves of the E bodies in figure 7 are shifted to the left). This result was particularly noticeable in composition 2, formulated with the highest amount of clay. As explained below, the different microstructures obtained by pressing or extruding ceramics could explain this fact [34], [35]. However, this difference tended to decrease (the pore size distribution curves of the P3 and E3 bodies almost coincide) when starch was added to the initial compositions, as a consequence of the drastic change in microstructure developed by the starch burnout [20], [28], [41]–[44]. With regard to open porosity, no significant differences associated with the shaping process were found. These findings confirm that i) the forming process of clayey compositions strongly affects the sintered piece microstructure and ii) this effect is to a large extent compensated by the addition of the organic pore former.

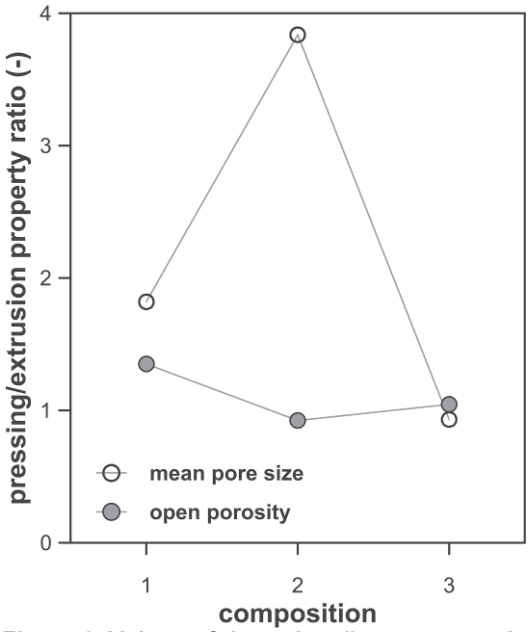

Figure 8. Values of the ratios: i) mean pore size (d_{50}) of P pieces/mean pore size (d_{50}) of E pieces and ii) open porosity of P pieces/open porosity of E pieces for the two series of bodies sintered at 60 min dwell time.

Micrographs of polished sections of P and E series samples are shown in figure 9. These pictures confirm many of the findings set out above concerning the pore size distribution of the membranes. The increase in soaking time for both pressing (P1) and extruding (E1) membranes from 6 min to 60 min gives rise to an evolution of the sintering process in terms of porosity reduction and above all of pore size coarsening. However, the most significant aspect revealed by the micrographs relates to composition 2, i.e. the sample with the highest clay content. As can be observed, the microstructure of the E2 specimen is clearly different from that of the P2 sample. The E2 microstructure is characterised by an orientated pore distribution, which follows a helical profile as a consequence of the movement of the colloidal clay particles travelling through the extruder auger. In addition, despite the large amount of pores, their connectivity is scarce. This microstructure has been extensively reported in the literature for typical heavy clay products manufactured by extrusion [36], [46]. It is also noticeable that the pore size of the E2 sample is much smaller than that of the P2 sample, which confirms the observation shown above. These microstructural differences are also observed with the P1 and E1 samples, which were formulated with lower amounts of clay, although the clay orientation is not so visible. In contrast, the addition of starch completely changes the microstructure of the extruded (E3) specimen, which looks much more like that of the pressed (P3) sample, confirming again the findings relating to the pore size distributions. It is noteworthy that the addition of the starch leads to increased porosity and pore size as well as enhancing pore connectivity, presumably resulting in much better membrane permeability. The effect of starch addition on membrane microstructure has been previously described in the membrane literature. Some authors have reported that starch additions higher than 10% give rise to a significant increase in the amount of interconnected pores created by starch burnout [28], [47], [48]. In summary, we can say that the effect of starch addition on the sintered microstructure of clayey compositions manages to counteract the impaired effect (lower porosity, smaller pore size and poor pore interconnectivity) produced by the clay content, even in the case of pieces shaped by extrusion in which the clayey particles are clearly orientated.

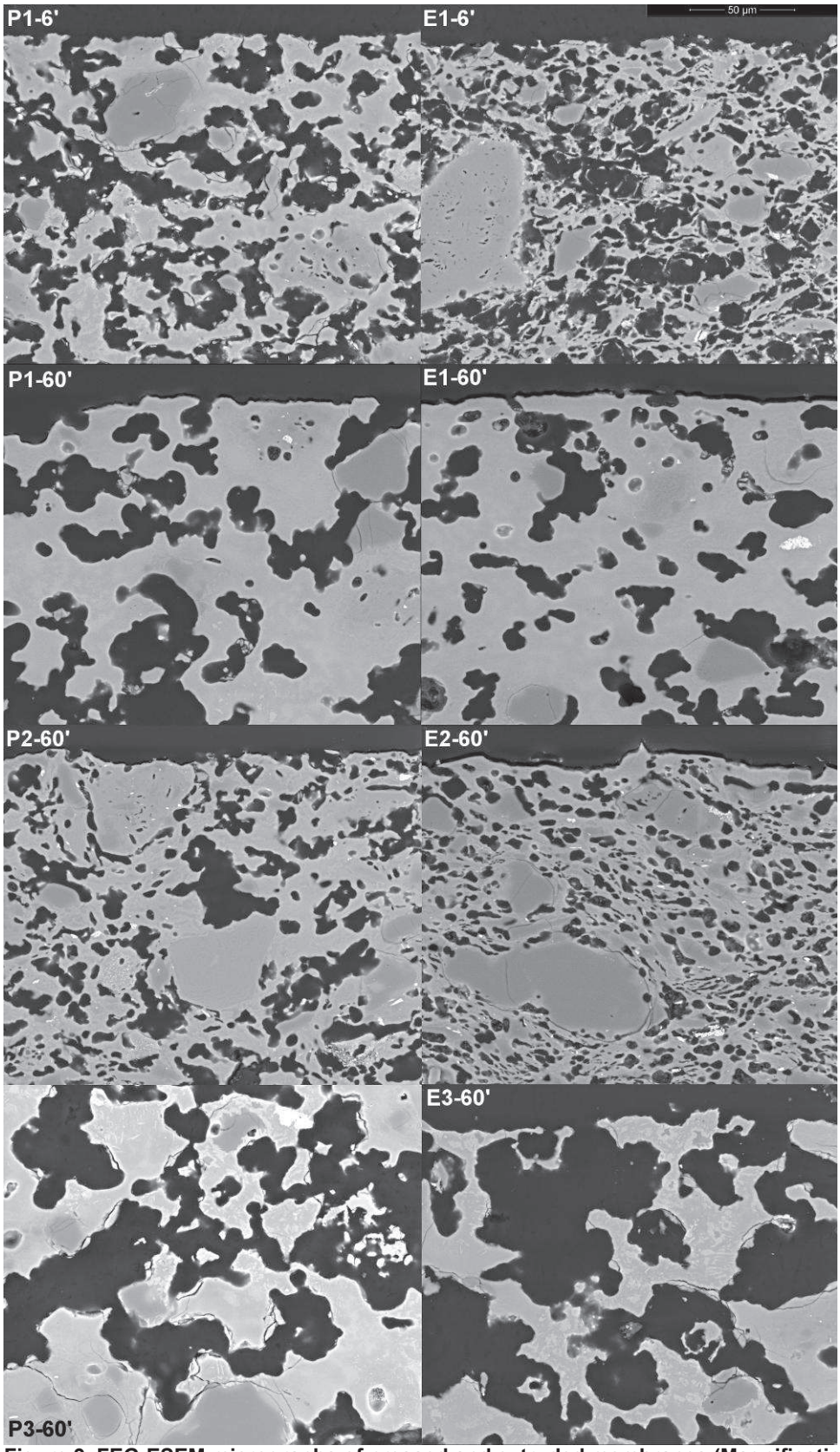

Figure 9. FEG-ESEM micrographs of pressed and extruded membranes (Magnification: 1500x). Standard composition pieces (P1 and E1) are shown for the two sintering cycles tested (6 min and 60 min of dwell time at maximum sintering temperature).

The mechanical strength of the membranes decreased with the increase in their porosity, as expected (Table 3). A comparison with the data in the literature shows that

the mechanical strength values are consistent with those reported previously, in the interval between 3 and 46 MPa [4], [26], [52], [57]. The mechanical strength showed an exponential relation with porosity (figure10) that agrees with the behaviour of other types of ceramic bodies [53]–[56]. The exponential trend is relatively well-defined bearing in mind that there were significant changes in the starting compositions of the raw materials as well as two different shaping methods. The findings reveal that mechanical strength is mainly related to the porosity of the membrane, which in turn is influenced by the starting composition, the shaping method and the soaking time.

Table 3. Mechanical strength of the sintered membranes.

Composition / Dwell time	Mechanical strength (MPa)	
	Pressed	Extruded
1 / 6’	32.0 ± 1.5	32.0 ± 1.6
1 / 60’	32.1 ± 1.4	39.7 ± 1.9
2 / 60’	32.0 ± 1.5	34.4 ± 1.8
3 / 60’	11.2 ± 0.5	13.1 ± 0.6

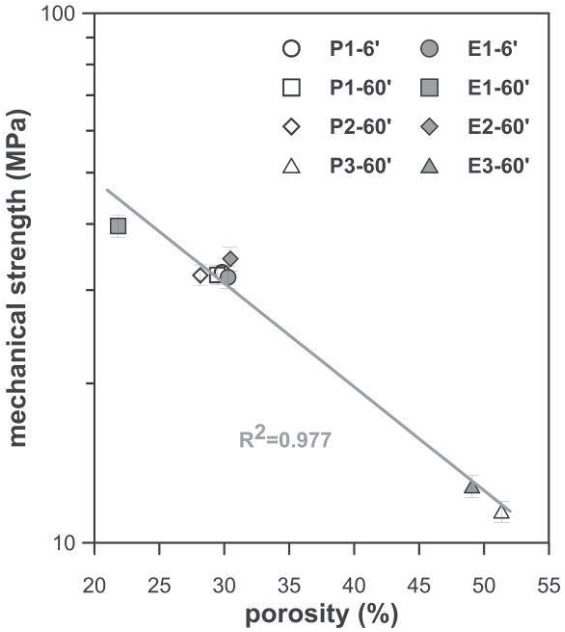

Figure 10. Mechanical strength versus open porosity for the two series of bodies sintered at 6 or 60 min dwell time. Continuous line plots the exponential fit.

3.3 Membrane functional characterization

The water permeability of all the samples (P and E series) was determined using the apparatus displayed in figure 4. Table 4 shows the water permeability values of all the sintered membranes.

Table 4. Water permeability of the sintered membranes.

Composition / Dwell time	Water permeability K_p $(m^2)\cdot10^{-16}$		Water permeability P_e $(L\cdot h^{-1}\cdot m^{-2}\cdot bar^{-1})$	
	Pressed	Extruded	Pressed	Extruded
1 / 6’	1,220	123	6,200	450
1 / 60’	3,100	390	15,800	1,480
2 / 60’	710	-	3,800	-
3 / 60’	25,240	9,050	45,700	34,900

The water permeability values showed considerable variations ranging from $123 \cdot 10^{-16}$ to $25{,}240 \cdot 10^{-16}$ m^2 (which corresponds to 450 to 45,700 $L \cdot h^{-1} \cdot m^{-2} \cdot bar^{-1}$). The lowest value was found for the extruded E2 sample, which contained the largest amount of clay. In fact, this membrane could not be measured in the apparatus due to its very low permeability (the lowest range of the permeameter is around 30 $L \cdot h^{-1} \cdot m^{-2} \cdot bar^{-1}$). The highest permeability value corresponded to the pressed sample containing starch (membrane P3). According to Mulder [49], the permeability values of commercial microfiltration ceramic oxide membranes are higher than 50 $L \cdot h^{-1} \cdot m^{-2} \cdot bar^{-1}$, but other authors have reported much higher values ranging from 300 to 50,000 $L \cdot h^{-1} \cdot m^{-2} \cdot bar^{-1}$, depending on the membrane pore size [38], [50]–[52]. Hence, some of the membranes developed in this work show permeability values in the same range than those of the most permeable membranes reported by literature.

In an attempt to correlate water permeability with the microstructural features (porosity and mean pore size) of ceramic membranes, the Hagen-Poiseuille relation was used (Eq.2), where K_p is the water permeability constant (m^2), d is the pore diameter (m), μ is the water viscosity (0.001 kg m^{-1} s^{-1}, at 20ºC and 1atm), ε_{sf} is the surface porosity (dimensionless) and τ is the tortuosity factor (dimensionless).

$$K_p = \frac{\varepsilon_{sf} \cdot d^2}{32 \cdot \mu \cdot \tau} \qquad \text{Eq. 2}$$

If the tortuosity of different membranes is considered similar, and considering ε_{sf} equals the open porosity obtained in the mercury intrusion porosimetry, equation 2 predicts a linear relationship between K_p and $(\varepsilon \cdot d^2)$ [20]. Figure 11 plots this correlation for all the samples (P and E series). For this representation, porosity and d_{50} from mercury pore sizing findings were used. It can be seen that the correlation is linear for all the samples, except for those samples with higher permeability (P3 and E3 sintered at 60 min dwell time, obtained by starch addition), which have not been included in figure 11. The permeability values confirm the previous results on microstructural features set out above using pore size distribution analysis and FEG-ESEM inspection. The fact that the P3 and E3 samples are far away from this correlation is not unexpected since these samples exhibit permeability values, which are at least one order of magnitude higher than those of the rest of the samples. Moreover, these findings confirm the effect of mean pore size on water permeability as well as the erroneous assumption of a constant tortuosity factor of the Hagen-Poiseuille equation for the different samples tested. This result is not surprising since a significant variation in the tortuosity can be expected for the samples obtained from different clay content and shaping methods. Differences in tortuosity are also suggested by the microstructural characterisation.

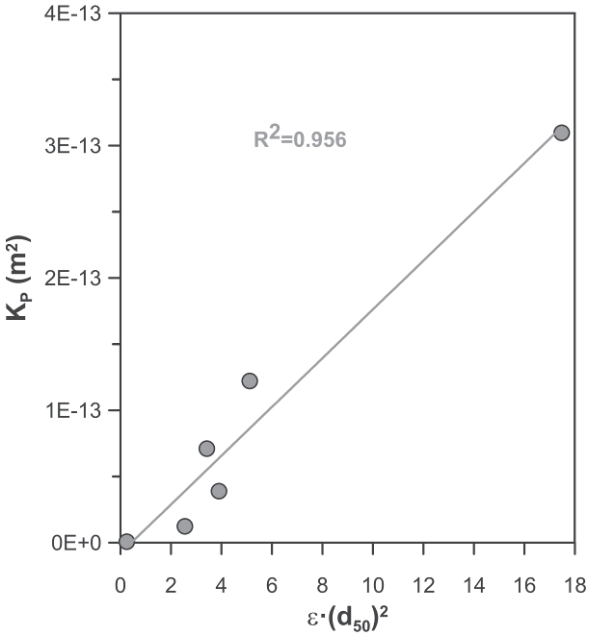

Figure 11. Plot of water permeability values (K_p) of all the membranes (P and E series) versus $\varepsilon \cdot d_{50}^2$ according to the Hagen-Poiseuille equation.

To better compare once again the extruded and pressed membranes, another ratio defined as P piece permeability/E piece permeability was calculated and then plotted in figure 12, together with the individual permeability values. The differences in permeability between the pressed and extruded membranes were very dependent on the composition nature, as set out above in the microstructural analysis. Hence, very clayey compositions shaped by extrusion resulted in membranes with very low permeability, while the addition of starch led to highly water-permeable membranes. These findings are consistent with the microstructural changes observed in figure 9.

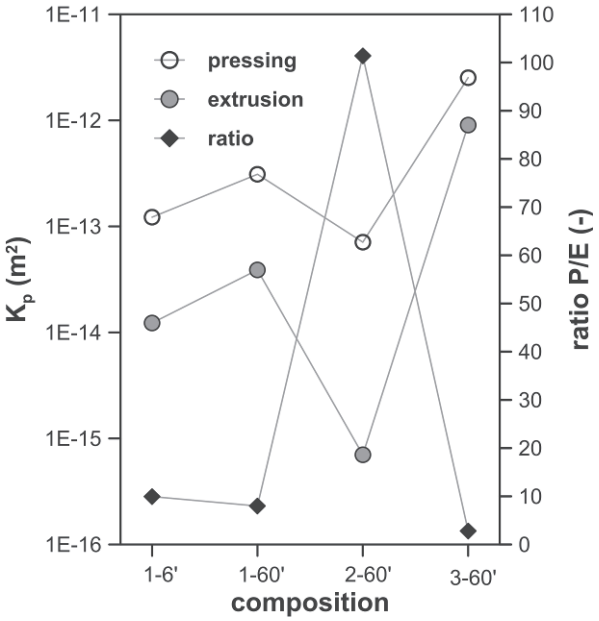

Figure 12. Values of permeabilities (K_p) and P piece permeability/E piece permeability ratio for the two series of bodies sintered at 6 and 60 min dwell time.

3.4 Tortuosity estimate from a proposed model

As stated above, the Hagen-Poiseuille equation, is usually employed to predict the water permeability of membranes [58]. Nevertheless, this equation uses the tortuosity factor (τ) which must be estimated by theoretical equations or empirical models [59]. In

this section the tortuosity factor is calculated by means of a simple model based on the Hagen-Poiseuille equation and the pore size distributions determined by mercury intrusion [60], [61] (see appendix).

According to the model described in the appendix, the tortuosity can be calculated from previously collected data. Using the described model, the tortuosities of the different samples were calculated and compiled in table 5.

Table 5. Tortuosities of the sintered membranes calculated by the proposed model set out in the appendix.

Composition / Dwell time	τ tortuosity factor (dimensionless)	
	Pressed	Extruded
1 / 6’	4.6	9.2
1 / 60’	2.5	2.8
2 / 60’	4.0	24.0
3 / 60’	1.5	2.4

The tortuosity values agreed well with the previous observations made by FEG-ESEM of the microstructure of the specimens, as described above. Firstly, the extruded membranes showed higher tortuosity values than those of the pressed membranes, as a consequence of their corresponding microstructures. Secondly, when the dwell time was increased from 6 to 60 minutes, a reduction in tortuosity was also observed for both the pressed and the extruded membranes owing to the sintering effects. Thirdly, the effect of the clay content of the starting composition on the resulting membrane microstructure was also confirmed from the results of composition 2 (with the highest amount of clay). The E2 body had the highest tortuosity value, due to the aforementioned orientation of clay particles during the extrusion process. Finally, when starch was added to the initial composition, the tortuosity decreased and the differences between both shaping methods were reduced, in agreement with the findings described in the previous sections.

4 Conclusions

It has been observed that, before sintering, the porosity of the extruded pieces was slightly lower than that of the pressed bodies obtained from the same low-cost composition. This difference can be attributed to the plastic properties of the clay, which readily forms a paste and can easily be extruded to the desired shape with lower extrusion pressure.

The membranes shaped by extrusion displayed, after sintering, less porosity and above all smaller pore sizes than those formed by dry pressing. This result became apparent as the clay content in the starting composition increased. The specific microstructure associated with the auger extrusion process was the main reason for this difference between the extruded and pressed membranes of the same composition. However, this difference tended to disappear when starch was added to the initial composition as a consequence of the drastic change in microstructure provided by the starch burnout. In addition, the mechanical strength of the membranes followed a decreasing exponential variation with porosity, which in turn was influenced by the starting composition, the shaping method and soaking time.

The water permeability showed a non-linear relationship with the specimen microstructure, as represented by the Hagen-Poiseuille term ($\varepsilon \cdot d^2$), ε and d being the porosity and mean pore size of the membrane, respectively. This variation highlights

the effect of the mean pore size and the tortuosity factor on permeability. Hence, very clayey compositions shaped by extrusion resulted in low permeability membranes, while the addition of starch gave rise to highly permeable membranes. The permeability values agreed with those reported in the literature. Moreover, a model has been derived from the Hagen-Poiseuille equation, which allows the estimation of the tortuosity values of the membranes. These calculated tortuosities are consistent with the microstructural features of the different specimens.

It is worth mentioning that the membranes developed in this work will be employed as supports of multilayer ceramic membranes for ultra and nanofiltration by developing thinner, selective layers, which will be addressed in future research.

5 Acknowledgements

This material is based upon work supported by the Spanish Ministry of Science and Innovation through the National Plan for Scientific Research, Development and Technology Innovation 2008-2011 (INNPACTO programme, project IPT-2011-1069-310000).

The authors wish to thank the personnel of FACSA (Fomento Agricola Castellonense S.A., Castellón, Spain), especially José Guillermo Berlanga, Ernesto Santateresa and Anna Gozalbo for their helpful aid and discussion during the execution of the present work.

6 References

[1] Baker RW. Membrane technology and applications. 2nd ed. Chichester: Wiley, 2004.
[2] Mallada R, Menéndez M. Inorganic membranes synthesis, characterization and applications. 1st ed. Oxford: Elsevier B.V., 2008.
[3] Burggraf AJ, Cot L. Fundamentals of Inorganic Membranes, Science and Technology. Amsterdam: Elsevier, 1996.
[4] Bouzerara F, Harabi A, Achour S, Larbot A. Porous ceramic supports for membranes prepared from kaolin and doloma mixtures. J Eur Ceram Soc 2006; 26:1663–71. http://dx.doi.org/10.1016/j.jeurceramsoc.2005.03.244
[5] Akhtar F, Rehman Y, Bergström L. A study of the sintering of diatomaceous earth to produce porous ceramic monoliths with bimodal porosity and high strength. Powder Technol 2010; 201:253–7. http://dx.doi.org/10.1016/j.powtec.2010.04.004
[6] Bejjaoui R, Benhammou A, Nibou L, Tanouti B, Bonnet JP, Yaacoubi A et al. Synthesis and characterization of cordierite ceramic from Moroccan stevensite and andalusite. Appl Clay Sci 2010; 49:336–40. http://dx.doi.org/10.1016/j.clay.2010.06.004
[7] Dong Y, Feng X, Feng X, Ding Y, Liu X, Meng G. Preparation of low-cost mullite ceramics from natural bauxite and industrial waste fly ash. J Alloys Compd 2008; 460:599–606. http://dx.doi.org/10.1016/j.jallcom.2007.06.023
[8] Dong Y, Hampshire S, Zhou J, Lin B, Ji Z, Zhang X, Meng G. Recycling of fly ash for preparing porous mullite membrane supports with titania addition. J Hazard Mater 2010; 180:173–80. http://dx.doi.org/10.1016/j.jhazmat.2010.04.010
[9] Zhou J, Zhang X, Wang Y, Larbot A, Hu X. Elaboration and characterization of tubular macroporous ceramic support for membranes from kaolin and dolomite. J Porous Mater 2010; 17:1–9. http://dx.doi.org/10.1007/s10934-008-9258-z
[10] Weir M, Rutinduka E, Detellier C. Fabrication, characterization and preliminary testing of all-inorganic ultrafiltration membranes composed entirely of a naturally occurring sepiolite clay mineral. J Membr Sci 2001; 182:41–50.
[11] Dong Y, Chen S, Zhang X, Yang J, Liu X, Meng G. Fabrication and characterization of low cost tubular mineral-based ceramic membranes for micro-

filtration from natural zeolite. J Membr Sci 2006; 281:592–9. http://dx.doi.org/10.1016/j.memsci.2006.04.029
[12] Le Van Mao R, Rutinduka E, Detellier C, Gougay P, Hascoet V, Tavakoliyan S et al. Mechanical and pore characteristics of zeolite composite membranes. J Mater Chem 1999; 9:783–8. http://dx.doi.org/10.1039/a806624h
[13] Harabi A, Zenikheri F, Boudaira B, Bouzerara F, Guechi A, Foughali L. A new and economic approach to fabricate resistant porous membrane supports using kaolin and $CaCO_3$. J Eur Ceram Soc 2014; 34:1329–40. http://dx.doi.org/10.1016/j.jeurceramsoc.2013.11.007
[14] Fakhfakh S, Baklouti S. Elaboration and characterisation of low cost ceramic support membrane. Adv Appl Ceram 2010; 109:31–8. http://dx.doi.org/10.1179/174367609X422234
[15] Anbri Y, Tijani N, Coronas J, Mateo E, Menéndez M, Bentama J. Clay plane membranes: development and characterization. Desalination 2008; 221:419–24. http://dx.doi.org/10.1016/j.desal.2007.01.101
[16] Khemakhem S, Larbot A, Ben Amar R. Study of performances of ceramic microfiltration membrane from Tunisian clay applied to cuttlefish effluents treatment. Desalination 2006; 200:307–9. http://dx.doi.org/10.1016/j.desal.2006.03.327
[17] Saffaj N, Persin M, Younsi SA, Albizane A, Cretin M, Larbot A. Elaboration and characterization of microfiltration and ultrafiltration membranes deposited on raw support prepared from natural Moroccan clay: Application to filtration of solution containing dyes and salts. Appl Clay Sci 2006; 31:110–9. http://dx.doi.org/10.1016/j.clay.2005.07.002
[18] Palacio L, Bouzerdi Y, Ouammou M, Albizane A, Bennazha J, Hernandez A et al. Ceramic membranes from Moroccan natural clay and phosphate for industrial water treatment. Desalination 2009; 245:501–7. http://dx.doi.org/10.1016/j.desal.2009.02.014
[19] Sánchez E, Mestre S, Pérez-Herranz V, Reyes H, Añó E. Membrane electrochemical reactor for continuous regeneration of spent chromium plating baths. Desalination 2006; 200:668–70. http://dx.doi.org/10.1016/j.desal.2006.03.475
[20] Sánchez E, Mestre S, Pérez-Herranz V, García-Gabaldón M. Síntesis de membranas cerámicas para la regeneración de baños de cromado agotados. Bol Soc Esp Ceram Vidr 2005; 44:409–14.
[21] Sánchez E, Mestre S, Pérez-Herranz V, García-Gabaldón M. Ceramic membranes for continuous regeneration of spent chromium plating baths. Key Eng Mater 2004;264–8: 2211–4.
[22] Abbasi M, Salahi A, Mirfendereski M, Mohammadi T, Rekabdar F, Hemmati M. Oily wastewater treatment using mullite ceramic membrane. Desalination Water Treat 2012; 37:21–30. http://dx.doi.org/10.1080/ 19443994.2012.661249
[23] García-Gabaldón M, Pérez-Herranz V, Sánchez E, Mestre S. Effect of tin concentration on the electrical properties of ceramic membranes used as separators in electrochemical reactors. J Membr Sci 2008; 323:213–20. http://dx.doi.org/10.1016/j.memsci.2008.06.039
[24] Nandi BK, Moparthi A, Uppaluri R, Purkait MK. Treatment of oily wastewater using low cost ceramic membrane: Comparative assessment of pore blocking and artificial neural network models. Chem Eng Res Des 2010; 88:881–92. http://dx.doi.org/10.1016/j.cherd.2009.12.005
[25] Belouatek A, Benderdouche N, Addaou A, Ouagued A, Bettahar N. Preparation of inorganic supports for liquid waste treatment. Microporous Mesoporous Mater 2005; 85:163–8. http://dx.doi.org/10.1016/j.micromeso.2005.06.007
[26] Nandi BK, Uppaluri R, Purkait MK. Preparation and characterization of low cost ceramic membranes for micro-filtration applications. Appl Clay Sci 2008; 42:102–10. http://dx.doi.org/10.1016/j.clay.2007.12.001
[27] Sahnoun RD, Baklouti S. Characterization of flat ceramic membrane supports prepared with kaolin-phosphoric acid-starch. Appl Clay Sci 2013; 83–4:399–404. http://dx.doi.org/10.1016/j.clay.2013.07.015

[28] Yang GCC, Tsai CM. Effects of starch addition on characteristics of tubular porous ceramic membrane substrates. Desalination 2008; 233:129–36. http://dx.doi.org/10.1016/j.desal.2007.09.035
[29] Majouli A, Tahiri S, Alami Younssi S, Loukili H, Albizane A. Elaboration of new tubular ceramic membrane from local Moroccan Perlite for microfiltration process. Application to treatment of industrial wastewaters. Ceram Int 2012; 38:4295–303. http://dx.doi.org/10.1016/j.ceramint.2012.02.010
[30] García-Ten J, Sánchez E, Amorós JL, García MC. Composiciones para la fabricación de baldosas cerámicas. Influencia de los distintos componentes sobre su comportamiento en el proceso de fabricación. Ceram Inf 1998; 243: 37–43.
[31] Beltrán V, Sánchez E, García-Ten J, Ginés F. Materias primas empleadas en la fabricación de baldosas de pasta blanca en España. Tec Ceram 1996; 241:114–28.
[32] Falamaki C, Naimi M, Aghaie A. Dual behavior of $CaCO_3$ as a porosifier and sintering aid in the manufacture of alumina membrane/catalyst supports. J Eur Ceram Soc 2004; 24:3195–201. http://dx.doi.org/10.1016/j.jeurceramsoc.2003.10.041
[33] Benito JM, Conesa A, Rodríguez MA. Membranas cerámicas. Tipos, métodos de obtención y caracterización. Bol Soc Esp Ceram Vidr 2004; 43:829–42.
[34] Carretero M, Dondi M, Fabbri B, Raimondo M. The influence of shaping and firing technology on ceramic properties of calcareous and non-calcareous illitic–chloritic clays. Appl Clay Sci 2002; 20:301–6.
[35] Reed JS. Principles of ceramics processing, 2nd Ed. New York, 1995.
[36] Krakowiak KJ, Lourenço PB, Ulm FJ. Multitechnique investigation of extruded clay brick microstructure. J Am Ceram Soc 2011; 94:3012–22. http://dx.doi.org/10.1111/j.1551-2916.2011.04484.x
[37] Biesheuvel PM, Verweij H. Design of ceramic membrane supports: permeability, tensile strength and stress. J Membr Sci 1999; 156:141–52.
[38] Pérez-Gálvez R, Guadix EM, Bergé JP, Guadix A. Operation and cleaning of ceramic membranes for the filtration of fish press liquor. J Membr Sci 2011; 384:142–8. http://dx.doi.org/10.1016/j.memsci.2011.09.019
[39] Chen Y, Burbidge A, Bridgwater J. Effect of carbohydrate on the rheological parameters of paste extrusion. J Am Ceram Soc 1997; 80:1841–50.
[40] Harabi A, Guechi A, Condom S. Production of Supports and Filtration Membranes from Algerian Kaolin and Limestone. Procedia Eng 2012; 33:220–4. http://dx.doi.org/10.1016/j.proeng.2012.01.1197
[41] Almeida FA, Botelho EC, Melo FCL, Campos TMB, Thim GP. Influence of cassava starch content and sintering temperature on the alumina consolidation technique. J Eur Ceram Soc 2009; 29:1587–94. http://dx.doi.org/10.1016/j.jeurceramsoc.2008.10.006
[42] Bazin MM, Ahmat MA, Zaidan N, Ismail AF, Ahmad N. Effect of starch addition on microstructure and strength of ball clay membrane. J Teknologi (Sciences Eng) 2014; 69:117–120.
[43] Sales S, Lorente-Ayza MM, Gilabert Albiol J, Sánchez E, Mestre S. Efecto de las características del almidón sobre la permeabilidad de las membranas cerámicas. Proceedings of the XIII Congreso Nacional de Materiales; 2014 June 18-20; Barcelona, Spain.
[44] Gregorová E, Pabst W, Bohačenko I. Characterization of different starch types for their application in ceramic processing. J Eur Ceram Soc 2006; 26:1301–9. http://dx.doi.org/10.1016/j.jeurceramsoc.2005.02.015
[45] Lorente-Ayza MM, Orts MJ, Pérez-Herranz V, Mestre S. Role of starch characteristics in the properties of low-cost ceramic membranes. J Eur Ceram Soc 2015; 35:2333–41. http://dx.doi.org/10.1016/j.jeurceramsoc.2015.02.026
[46] Maillard P, Aubert JE. Effects of the anisotropy of extruded earth bricks on their hygrothermal properties. Constr Build Mater 2014; 63:56–61. http://dx.doi.org/10.1016/j.conbuildmat.2014.04.001

[47] Alves HM, Tarì G, Fonseca AT, Ferreira JMF. Processing of porous cordierite bodies by starch consolidation. Mater Res Bull 1998; 33: 1439–48.
[48] Lyckfeldt O, Ferreira JMF. Processing of Porous Ceramics by 'Starch Consolidation. J Eur Ceram Soc 1998; 18:131–140.
[49] Mulder M. Basic Principes of Membrane Technology. 2nd ed. Dordrecht: Kluwer Academic Publishers, 1996.
[50] Majouli A, Tahiri S, Alami Younssi S, Loukili H, Albizane A. Treatment of effluents coming from beamhouse section of tannery by microfiltration through Cordierite/Zirconia and Alumina tubular ceramic. J Mater Environ Sci 2012; 3:808–15.
[51] Scott K. Handbook of Industrial Membranes, 2nd ed. Oxford, 1999.
[52] Vasanth D, Pugazhenthi G, Uppaluri R. Fabrication and properties of low cost ceramic microfiltration membranes for separation of oil and bacteria from its solution. J Membr Sci 2011; 379:154–63. http://dx.doi.org/10.1016/j.memsci.2011.05.050
[53] Amorós JL, Feliu C, Ginés F, Agramunt JV. Resistencia mecánica y microestructura de soportes cerámicos en crudo. Proceedings of the Qualicer'96-IV Congreso Mundial de la Calidad del Azulejo y del Pavimento Cerámico; 1996 March 10-13; Castellón, Spain.
[54] Negre F, Sánchez E, Ginés F, García-Ten J, Feliu C. Procedimiento experimental para determinar la resistencia mecánica mediante flexión por tres puntos de apoyo. Tec Ceram 1996; 225:452–63.
[55] Jordán Vidal MM, Sanfeliu Montolio T, De La Fuente Cullell C. Resistencia mecánica y porosidad de soportes para pavimentos y revestimientos cerámicos obtenidos con arcillas de Castellón. Mater Constr 2001; 261:5–20.
[56] Amorós JL, Feliu C, Ginés F, Agramunt JV. Resistencia mecánica y microestructura de soportes cerámicos en crudo. Tec Ceram 1996; 244:362–75
[57] Monash P, Pugazhenthi G. Development of ceramic supports derived from low-cost raw materials for membrane applications and its optimization based on sintering temperature. Int J Appl Ceram Technol 2011; 8:227–38. http://dx.doi.org/10.1111/j.1744-7402.2009.02443.x
[58] Li W, Xing W, Xu N. Modeling of relationship between water permeability and microstructure parameters of ceramic membranes. Desalination 2006; 192:340–5. http://dx.doi.org/10.1016/j.desal.2005.07.042
[59] Shen L, Chen Z. Critical review of the impact of tortuosity on diffusion. Chem Eng Sci 2007; 62:3748–55. http://dx.doi.org/10.1016/j.ces.2007.03.041
[60] Sales S. Intercambiadores iónicos inorgánicos nanoestructurados: síntesis e infiltración en membranas cerámicas. Ph.D thesis 2015; Universitat Jaume I.
[61] Gilabert J. Relación del coeficiente de permeabilidad de membranas cerámicas con las condiciones de síntesis. MSc thesis 2012; Universitat Jaume I.

APPENDIX

The Hagen-Poiseuille equation assumes that liquid circulates through a beam of parallel cylindrical pores, which cross the membrane from one side to the other (eq. A.1), where J is the flux through the membrane ($m^3 \cdot s$), ΔP is the drop pressure through the membrane (Pa), r is the pore radius (m), n is the number of pores, μ is the water viscosity (Pa·s) and L is the pore length, that is considered equal to the membrane thickness (m).

$$J = -n \cdot \frac{\pi \cdot r^4}{8 \cdot \mu \cdot L} \cdot \Delta P \qquad \text{Eq. A.1}$$

To calculate n, the most difficult variable to determine, it was considered that membranes can be modelled by a beam of parallel cylindrical pores of different diameters. It is assumed that a pore volume V_{Pd} exists for every value of a determined pore of radius r. Thus, n(r) is the factor between the volume of pores with radius r and the volume of one pore:

$$n(r) = \frac{V_{P_d}(r)}{\pi \cdot r^2 \cdot L} \qquad \text{Eq. A.2}$$

The mercury pore sizing technique allows the pore size distribution to be calculated assuming that all the pores are cylindrical with a radius r. The result is the curve: accumulated pore volume $V_{Pa}(r)$ by mass unit versus pore radius. By deriving this curve, the differential pore volume for every radius is obtained ($V_{Pd}(r)$):

$$V_{P_a}(r) = \int_{r_i}^{r} V_{P_d}(r)dr \qquad \text{Eq. A.3} \qquad \text{-->} \qquad V_{P_d}(r) = \frac{dV_{P_a}(r)}{dr} \qquad \text{Eq. A.4}$$

On the other hand, mercury pore sizing findings provide pairs of data [r, V_{Pa}] which can not be easily adjusted to a determined function; nevertheless, blocks of 3 points can be adjusted to a parabola (Simpson integration method) and the cumulative and differential curves can be defined, whose constants depend on the experimental data used to calculate them.

$$V_{P_d}(r) = ar^2 + br + c \qquad \text{Eq. A.5} \qquad \text{-->} \qquad V_{P_d}(r) = 2ar + b \qquad \text{Eq. A.6}$$

Introducing equation A.6 in equation A.2:

$$n(r) = \frac{V_{P_d}(r)}{\pi \cdot r^2 \cdot L} = \frac{2ar + b}{\pi \cdot r^2 \cdot L} \qquad \text{Eq. A.7}$$

Replacing the n(r) estimation (equation A.7) in the Hagen-Poiseuille equation (equation A.1) and integrating the resulting expression, an equation to calculate the flux through the membrane (J) is obtained:

$$J = \frac{\Delta P}{8 \cdot \mu \cdot L^2} \cdot \sum_{i=1}^{m} \left[\frac{a_i}{2} \left(r_{i_{\max}}^4 - r_{i_{\min}}^4 \right) + \frac{b_i}{3} \left(r_{i_{\max}}^3 - r_{i_{\min}}^3 \right) \right] \qquad \text{Eq. A.8}$$

Since pores are neither cylindrical nor straight and possess tortuosity, the actual pore length is defined as the product of the membrane thickness (L_m) and the tortuosity:

$$J = \frac{\Delta P}{8 \cdot \mu \cdot \tau^2 \cdot L_m^2} \cdot \sum_{i=1}^{m} \left[\frac{a_i}{2} \left(r_{i_{\max}}^4 - r_{i_{\min}}^4 \right) + \frac{b_i}{3} \left(r_{i_{\max}}^3 - r_{i_{\min}}^3 \right) \right] \qquad \text{Eq. A.9}$$

In equation A.9, all the variables are known and constant (cst), except the tortuosity:

$$J = \frac{cst}{\tau^2} \cdot \Delta P \qquad \text{Eq. A.10}$$

On the other hand, the water permeability test provides a constant (the straight line slope, slp) that relates water flux and drop pressure:

$$J = slp \cdot \Delta P \qquad \text{Eq. A.11}$$

Consequently, the tortuosity can then be calculated by means of the constant (cst) and the slope (slp):

$$\tau = \sqrt{\frac{cst}{slp}} \qquad \text{Eq. A.12}$$